DEVELOPMENTAL BIOLOGY

Physiological ROS controls Upd3-dependent modeling of ECM to support cardiac function in *Drosophila*

Jayati Gera[1], Prerna Budakoti[1], Meghna Suhag[1]†, Lolitika Mandal[2], Sudip Mandal[1]*

Despite their highly reactive nature, reactive oxygen species (ROS) at the physiological level serve as signaling molecules regulating diverse biological processes. While ROS usually act autonomously, they also function as local paracrine signals by diffusing out of the cells producing them. Using in vivo molecular genetic analyses in *Drosophila*, we provide evidence for ROS-dependent paracrine signaling that does not entail ROS release. We show that elevated levels of physiological ROS within the pericardial cells activate a signaling cascade transduced by Ask1, c-Jun N-terminal kinase, and p38 to regulate the expression of the cytokine Unpaired 3 (Upd3). Upd3 released by the pericardial cells controls fat body–specific expression of the extracellular matrix (ECM) protein Pericardin, essential for cardiac function and healthy life span. Therefore, our work reveals an unexpected inter-organ communication circuitry wherein high physiological levels of ROS regulate cytokine-dependent modulation of cardiac ECM with implications in normal and pathophysiological conditions.

INTRODUCTION

Cellular metabolic processes that use molecular oxygen as the ultimate electron acceptor inevitably form a diverse array of highly reactive oxygen–derived radicals, collectively known as reactive oxygen species (ROS). The notable members of the ROS family include superoxide anion, hydrogen peroxide, hydroxyl radical, and singlet oxygen (*1*). Although mitochondrial oxidative phosphorylation is considered to be the primary contributor for cellular ROS, many ROS-producing enzymes, such as NADPH (reduced form of nicotinamide adenine dinucleotide phosphate) oxidase, xanthine oxidase, and endothelial nitric oxide synthase, also generate a substantial amount of ROS (*2*, *3*). Intriguingly, cells have evolved a sophisticated enzymatic antioxidant defense system that includes superoxide dismutase, catalase, and glutathione peroxidase for scavenging the ROS to maintain physiological redox homeostasis. However, when ROS production exceeds the buffering capacity of the antioxidant defense systems, cells experience "oxidative stress," which has been implicated either for the onset or for the progression of neurodegeneration, atherosclerosis, diabetes, metabolic disorders, carcinogenesis, and cardiovascular diseases (*4*). Notwithstanding the deleterious roles of ROS, there is now a greater understanding of their role as versatile pleiotropic signaling agents that impinge on normal physiological and redox responses. The physiological flux of ROS modulates several complex processes such as adaptation to hypoxia (*5*), immune responses (*6*), cognitive functions (*7*), regulation of blood pressure (*8*), organismal growth (*9*), differentiation of stem cells (*10*), wound healing (*11*), and even aging (*12*).

Studies in the recent past have documented a complex interplay between ROS and the extracellular matrix (ECM), with each modulating the other. It has been evidenced that integrin-mediated cell–ECM contact triggers ROS production (*13*) either by promoting changes in mitochondrial metabolic function (*14*) or by activating distinct oxidases, including NADPH oxidases (*15*, *16*). Conversely, ROS can influence the assembly and turnover of ECM at different levels. While ROS play an essential role in the degradation of ECM proteins by regulating the expression and activation of matrix metalloproteinases (*17*), ROS-dependent rearranging of inter- and intramolecular disulfide bridges within ECM proteins lead to activity-relevant conformational changes of the ECM (*18*). Furthermore, considering the indirect role of ROS in hypoxia-induced factor 1α (HIF1α) activation (*19*), it has been implicated in the transcriptional activation of several HIF1α-inducible genes that code for ECM components and enzymes involved in posttranslational modification of nascent matrix proteins (*20*). Besides their participation in regulated ECM remodeling, ROS can also elicit pathological processes like fibrosis by contributing to the unbalanced excess of ECM deposition in fibrotic tissues. ROS released by the infiltrating leukocytes and the resident mesenchymal cells at the inflammation site activates transforming growth factor–β1 (TGFβ1) to orchestrate the differentiation of fibroblasts to myofibroblast, an essential process for fibrosis (*21*, *22*). Notably, the involvement of ROS in modeling the ECM evidenced so far under both normal and pathophysiological conditions is restricted to the local environment wherein ROS is produced. Any evidence for the involvement of physiological ROS in long-range ECM remodeling is lacking.

The cardiac ECM is an essential component of the heart that imparts a tight spatiotemporal regulation of different cellular processes during cardiogenesis and homeostasis. The *Drosophila* heart has served as an excellent in vivo model to provide several important insights into how the cardiac ECM undergoes developmental remodeling to ensure tissue integrity and functionality. Proper assembly of the cardiac ECM around the heart not only is essential for cardiogenesis in the fly embryo but also aids in maintaining appropriate connections between cardiomyocytes and adjacent supporting cells such as the pericardial cells (PCs) and the alary muscles, restores diastolic heart diameter, and helps to synchronize cardiomyocyte contraction in the larval and adult stages (*23*). Pericardin (Prc), which displays certain homologies to mammalian collagen IV, is a unique component of the cardiac ECM in flies (*24*). Genetic evidence suggests that Prc promotes proper migration and alignment of heart cells during cardiogenesis and absence of *prc* or its ECM adaptor protein Lonely heart (Loh) (*23*) disrupts heart

[1]Molecular Cell and Developmental Biology Laboratory, Department of Biological Sciences, Indian Institute of Science Education and Research Mohali, Punjab 140306, India. [2]Developmental Genetics Laboratory, Department of Biological Sciences, Indian Institute of Science Education and Research Mohali, Punjab 140306, India.
*Corresponding author. Email: sudip@iisermohali.ac.in
†Present address: Department of Cell and Developmental Biology, Tel Aviv University, Tel Aviv 6997801, Israel.

integrity, eventually leading to luminal collapse and heart failure (*24*–*26*). However, despite having a vast literature endorsing that the assembly of a single ECM protein, such as Prc, is crucial for organ integrity, our knowledge about any regulatory mechanism for Prc production essential for cardiac homeostasis is still unmet.

Our quest for the mechanism that regulates Prc expression in adult flies establishes the role of the cytokine Unpaired 3 (Upd3), synthesized and released by the PCs, to control the fat body–specific expression of *pericardin*. We demonstrate that simultaneous activation of c-Jun N-terminal kinase (JNK) and p38 signaling in the PCs by physiological levels of ROS induce the expression of *upd3*. Thus, besides unfurling an otherwise unknown paradigm of complex inter-organ communication that links the metabolic states of the PCs in regulating cardiac function, the outcome of this study identifies another facet of ROS as a regulator of ECM remodeling under normal physiological conditions with far-reaching implications in the field of fibrosis.

RESULTS

The adult fat body cells synthesize Prc

The adult heart of *Drosophila*, also known as the cardiac tube (or dorsal vessel), is a contractile, linear, tubular structure spanning the entire abdomen underneath the dorsal cuticle. Anteriorly, it extends as the aorta that conducts hemolymph to the head capsule (Fig. 1A). The abdominal heart consists of a series of four chambers marked by incurrent ostia (arrows in Fig. 1B) responsible for the inflow of hemolymph into the heart. The lumen of the cardiac tube is enclosed by the cardiomyocytes and a series of PCs flank the cardiac tube on its either side (Fig. 1C). While pairs of alary muscles, which perform the role of a diaphragm, keep the heart suspended from the epidermis, the cardiac ECM, which includes Prc, surrounds the cardiac tube and maintains connection with the PCs and the alary muscles (Fig. 1C).

Previous studies have demonstrated that flies, homozygous mutants for *prc*, exhibit luminal collapse and heart failure primarily due to gradual irreversible detachment of PCs from the heart tube (*25*, *26*). In contrast, adult flies with one copy loss of *prc* ($prc^{MB03017}$/+) have an otherwise normal-looking cardiac tube with PCs attached to it (fig. S1A). However, the heterozygous mutants with 50% drop in the level of *prc* transcripts (fig. S1B) have reduced level of Prc accumulation around the heart (fig. S1, C to D′). Quantitative analysis reveals 50% reduction in the mean intensity of Prc accumulation around the second chamber of the heart of $prc^{MB03017}$/+ flies as compared to control (fig. S1E). Furthermore, compared to control flies of similar age, the heart of $prc^{MB03017}$/+ flies exhibits irregular beating patterns (fig. S1, F and G, and movies S1 and S2) with a significant increase in arrhythmia index (fig. S1H), and increased and irregular heart period (fig. S1I) due to an increase in both diastolic and systolic intervals (fig. S1, J and K). The life span of the *prc* heterozygous mutant flies is significantly reduced (fig. S1L) with the median survival being 19 days shorter than the control flies (fig. S1M). Put together, these results highlight the importance of Prc in regulating cardiac activity and its possible impact on the life span of adult flies.

Although it has been documented that the PCs serve as the source of Prc during embryogenesis (*24*), and larval Prc is synthesized and secreted by the fat body cells (*25*), our understanding about the source of Prc in adults is obscure. To determine that, we analyzed the reporter green fluorescent protein (GFP) expression in *Prc-Gal4; UAS-2XEGFP* flies. Distinct GFP expression is observed in the adult fat body (Fig. 1, D and E) but not in the PCs (arrowheads in fig. S1N). Knocking down *prc* expression, by *yolk-Gal4*, which expresses in the adult fat body (fig. S1O), causes a drastic drop in the level of *prc* transcript in the fat cells (fig. S1P). A reduction in the organismal Prc protein level (Fig. 1, F and F′) and that of Prc accumulation around the cardiac tube are also observed (Fig. 1, G to H′, and fig. S1Q). However, the organismal level of Prc protein remains unaltered upon knocking down *prc* specifically in the PCs by *dorothy-Gal4* (*dot-Gal4*) (fig. S1, R and R′). Furthermore, fat body–specific knocking down of the small guanosine triphosphatase Sar1 (essential for the formation of vesicles transport between endoplasmic reticulum and Golgi complex and subsequent protein secretion) (*27*) results in trapping of Prc within the fat cells (fig. S1, S and T) with a concomitant drop in the amount of Prc accumulation around the heart (Fig. 1, I and I′, and fig. S1Q). More than 50% reduction in the mean intensity of Prc accumulation around the second chamber of the heart, as compared to control, is observed upon attenuating the release of Prc from the fat cells (fig. S1Q). Flies wherein either the fat cell–specific *prc* expression has been down-regulated or the release of Prc from the fat cells has been blocked demonstrate irregular heartbeat (Fig. 1, J to L, and movies S3 to S5), with increased arrhythmia index (Fig. 1M), heart period (Fig. 1N), diastolic interval (Fig. 1O), and systolic interval (Fig. 1P). The observed changes resemble the cardiac dysfunctions detected in $prc^{MB03017}$/+ heterozygous mutants (fig. S1, H to K). Together, these results establish that, in adult flies, Prc, a critical regulator of cardiac function, gets synthesized and secreted by the fat cells.

Expression of *prc* in the adult fat body cells is regulated by JAK-STAT signaling

In silico analyses to determine the signaling pathway involved in activation of *prc* expression led to the identification of a consensus-binding site for signal transducer and activator of transcription (STAT), the transcription factor for Janus kinase (JAK)–STAT signaling pathway in the putative regulatory region of *prc* (arrow in Fig. 2A). Similar potential STAT binding sequence exists in at least five other species of *Drosophila*, upstream to the genes annotated to code for Collagen IV (Fig. 2A). The JAK-STAT signaling cascade is a highly conserved pathway regulating diverse cell biological processes across taxa (*28*). In flies, binding of any of the cytokine ligands (Upd1/Upd2/Upd3) to their cognate receptor, Domeless, leads to activation of JAKs by transphosphorylation. Subsequent phosphorylation of STATs, by activated JAK, results in STAT dimerization and their nuclear translocation to regulate target gene expression (Fig. 2B) (*29*).

To ascertain the involvement of JAK-STAT signaling in regulating *prc* expression, we first checked for STAT activity in the fat body. As evident from Fig. 2C, the adult fat cells express the reporter for STAT activity (10XStat92E-GFP) (*30*). Attenuating the JAK-STAT signaling by knocking down the expression of either Stat92E or Domeless in the fat body results in a drastic drop in the level of *prc* transcripts (Fig. 2D) and is accompanied by less deposition of Prc around the cardiac tube (Fig. 2, E to G). Conversely, fat body–specific overexpression of Stat92E causes a detectable increase in *prc* expression (Fig. 2D) and increased accumulation of Prc around the cardiac tube (fig. S2, A and G). Affecting the deposition of Prc around the cardiac tube, either way, generates irregular heartbeats (Fig. 2, H to J, and movies S6 to S8) with increased arrhythmia index (Fig. 2K).

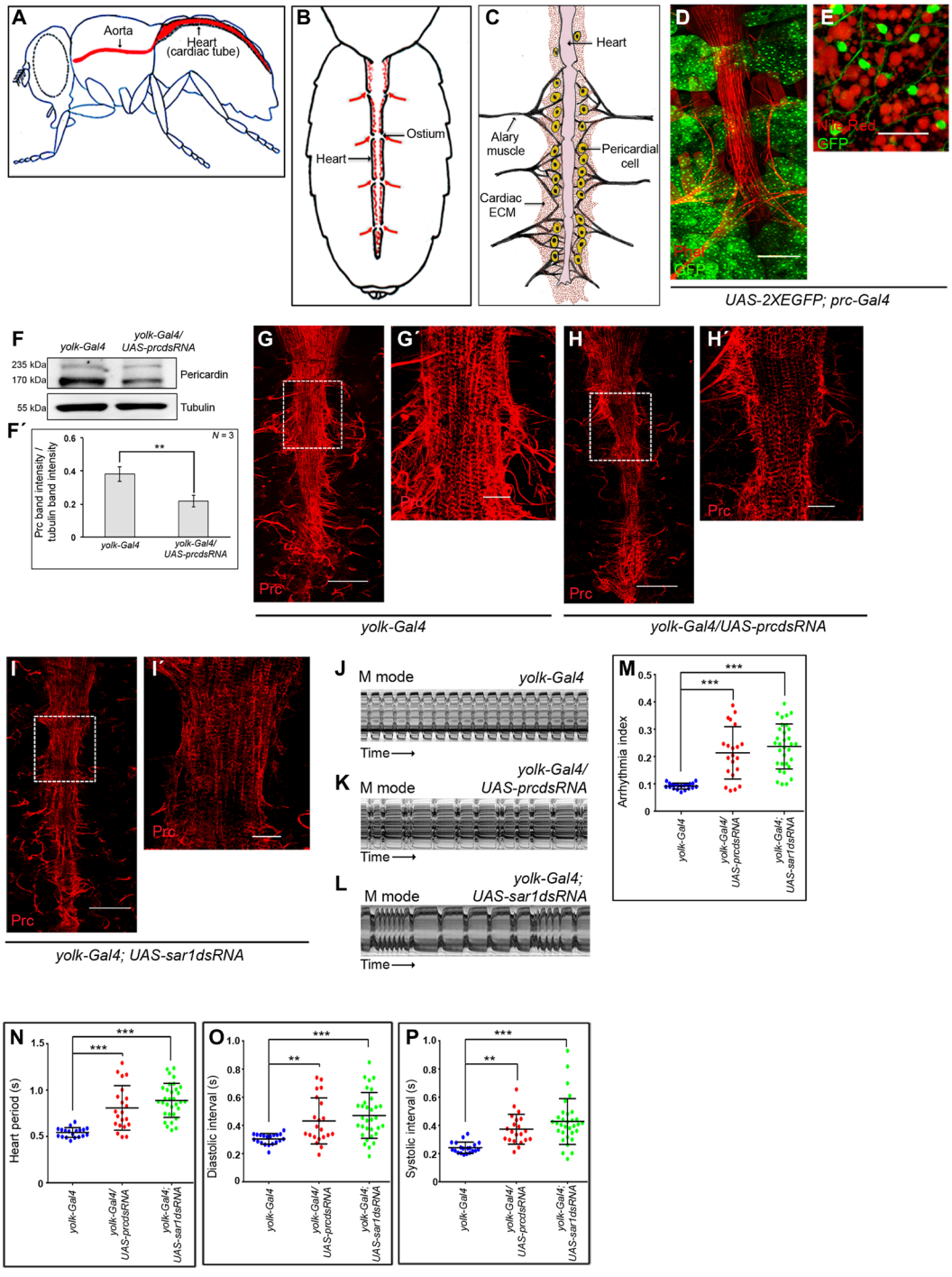

Fig. 1. Adult fat cells express and release Prc to regulate cardiac function. (**A** and **B**) Schematic representations showing the anatomical position of the adult heart (A) and that of the four cardiac chambers (B) in *Drosophila*. Arrows mark the directionality of the inflow of hemolymph. (**C**) Diagram showing the adult heart of *Drosophila* and the cardiac ECM. (**D** and **E**) Reporter GFP expressions for *prc* (green) in the adult fat cells. Lipid droplets (red) are marked in the high-magnification image (E). Scale bars, 100 μm (D) and 20 μm (E). (**F** and **F´**) Immunoblot analysis demonstrating reduction in organismal Prc level upon knocking down *prc* in adult fat cells. Tubulin serves as the loading control (F). Quantification of the Prc band intensities normalized to that of tubulin band intensities (F´). (**G** to **I´**) Knocking down either *prc* (H) or *sar1* (I) in the fat cells decreases the level of Prc (red) accumulation around the heart as compared to control (G). (G´), (H´), and (I´) represent zoomed-in images of the second heart chamber marked with a box in (G), (H), and (I), respectively. Scale bars, 100 μm (G, H, and I) and 25 μm (G´, H´, and I´). (**J** to **L**) Representative M-mode records for heartbeats of adult flies showing the movement of the heart tube walls (*y* axis) over time (*x* axis). (**M** to **P**) Changes in Arrhythmia Index (M), Heart Period (N), Diastolic Interval (O), and Systolic Interval (P) upon knocking down either *prc* or *sar1* in the fat cells. The dots represent the samples analyzed for each genotype. Genotypes are as mentioned. Data are presented as means ± SD. Statistical significance with *P* values of $P < 0.01$, and $P < 0.001$ are mentioned as **, and ***, respectively. ns, not significant.

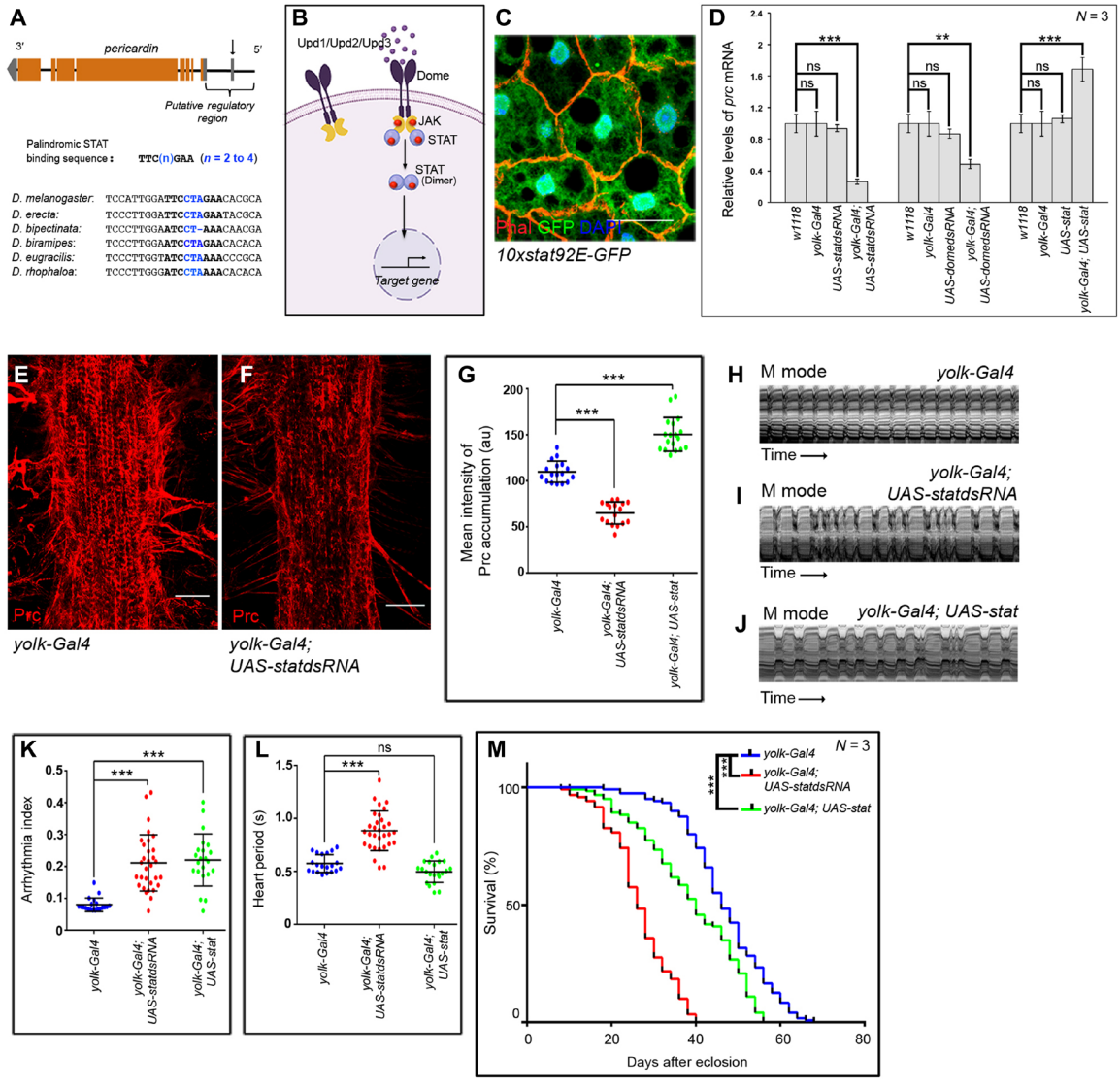

Fig. 2. JAK-STAT signaling regulates *prc* expression in the fat body cells. (**A**) Schematic representation of *prc* genomic region (not up to scale) of *Drosophila melanogaster*, marking the potential STAT-binding site (arrow). Sequence alignment of the regulatory regions of the annotated genes coding for Collagen IV in different species of *Drosophila* highlighting the conserved potential STAT-binding site. (**B**) Schematic representation of the JAK-STAT signaling pathway in *Drosophila*. (**C**) Expression for *10xStat92EGFP* (green) in adult fat cells. Phalloidin (red) marks the cell boundaries and DAPI (4′,6-diamidino-2-phenylindole) (blue) marks the nuclei. Scale bar, 20 μm. (**D**) Changes in *prc* expression upon modulating JAK-STAT signaling in fat cells. The transcript levels are normalized to that of the constitutive ribosomal gene *rp49*. (**E** and **F**) Down-regulating *stat92E* in fat cells reduces the level Prc accumulation around the second heart chamber (F) as compared to control (E). Scale bars, 25 μm. (**G**) Quantification of the mean fluorescence intensity for Prc accumulation around the second heart chamber upon modulating *stat92E* in fat cells. The dots represent the samples analyzed for each genotype. au, arbitrary units. (**H** to **J**) Representative M-mode records for heartbeats of adult flies showing the movement of the heart tube walls (*y* axis) over time (*x* axis). (**K** and **L**) Changes in Arrhythmia Index (K) and in Heart Period (L) upon modulating JAK-STAT signaling in adult fat cells. The dots represent the samples analyzed for each genotype. (**M**) Survival rates of *yolk-Gal4; UAS-statdsRNA* and *yolk-Gal4; UAS-stat* flies as compared to that of the control *yolk-Gal4* flies. Genotypes are as mentioned. Data are represented as means ± SD. Statistical significance with *P* values of $P < 0.01$, and $P < 0.001$ are mentioned as **, and ***, respectively.

While the diastolic interval is affected in both the conditions (fig. S2B), changes in heart period (Fig. 2L) and systolic interval (fig. S2C) are more apparent in cardiac tubes with less Prc around them. Furthermore, life-span analyses of these flies emphasize the requirement for optimal level of Prc accumulation around the cardiac tube to support normal life span. Flies with either reduced or increased amount of Prc in the cardiac ECM demonstrate reduced life span (Fig. 2M). The median life span of the flies with decreased or increased amount of Prc are shorter than that of the control by 19 and 8 days, respectively (fig. S2D). Put together, these results highlight the role of Stat92E as a transcriptional regulator of *prc* expression in the fat body and emphasize the importance of optimal amount of Prc for normal cardiac function and life span.

Next, we sought to determine whether increased expression of *prc* caused by overexpressing *Stat92E* in the fat cells (refer to Fig. 2D) could restore the cardiac dysfunction and reduced life span of $prc^{MB03017}$/+ flies. As evident from Fig. 3A, overexpressing *Stat92E* in the fat cells causes an appreciable increase in the *prc* transcript

level of $prc^{MB03017}$/+ flies. Concurrent with this result, a significant recovery in the amount of Prc accumulation around the cardiac tube is observed (Fig. 3, B to E). Furthermore, although a detectable suppression of the irregularity in the heartbeats of $prc^{MB03017}$/+ flies is observed upon compensating the amount of Prc accumulation in the cardiac ECM (fig. S2, E to G, and movie S9), the heart still beats at a slower rate as compared to that observed in control flies. A significant recovery in arrhythmia index (Fig. 3F), heart period (Fig. 3G), diastolic interval (fig. S2H), and systolic interval (fig. S2I) is observed. Overexpression of *prc* not only restores the cardiac dysfunction of $prc^{MB03017}$/+ flies but also brings about significant recovery in their life span. While both $prc^{MB03017}$/+ and *yolk-Gal4; UAS-stat* flies demonstrate appreciable reductions in their life span when compared to that of control w^{1118} and *yolk-Gal4* flies, restoration of *prc* expression by overexpression of *Stat92E* in the fat cells results in a remarkable recovery in the life span of *yolk-Gal4; UAS-stat/*$prc^{MB03017}$ flies (Fig. 3H). The magnitude of this recovery becomes further evident upon performing median survival analyses. Overexpression of *prc* leads to a notable restoration of the drop in the median survival of $prc^{MB03017}$/+ flies, with the median survival of *yolk-Gal4; UAS-stat/*$prc^{MB03017}$ flies being comparable to that of the control flies (fig. S2J). Together, apart from establishing that the JAK-STAT signaling is required and sufficient to induce *prc* expression, these results provide the genetic link that connects optimal amount of Prc accumulation in the cardiac ECM with normal cardiac function and life span.

Upd3, released by the PCs, regulates *prc* expression in the fat body

Members of the Unpaired family of proteins, Upd1, Upd2, and Upd3, constitute the ligands of the JAK-STAT pathway. To analyze the ligand responsible for triggering *prc* expression, we first checked for the expression of *prc* in the fat body of flies that are bona fide mutants for any of the unpaired genes. *upd1* homozygous mutants ($upd1^{YM55}$/$upd1^{YM55}$) (*31*) being embryonic lethal, we probed for *prc* expression in heterozygous mutants of *upd1* ($upd1^{YM55}$/*FM7*). Flies, homozygous null mutants for either *upd2* ($upd2^{\Delta}$/$upd2^{\Delta}$) or *upd3* ($upd3^{\Delta}$/$upd3^{\Delta}$) (*32*), were also analyzed for *prc* expression. Compared to a modest drop in the level of *prc* expression in the fat body of either $upd1^{YM55}$/*FM7* or $upd2^{\Delta}$/$upd2^{\Delta}$flies (Fig. 4A), a robust drop in *prc* expression is detected in the fat body of $upd3^{\Delta}$/$upd3^{\Delta}$ homozygous null mutant flies (Fig. 4A).

In the next set of experiments, we independently down-regulated the expression of *upd1* or *upd2* or *upd3* in different adult tissues and assayed for *prc* expression in the fat body. While no appreciable drop in *prc* expression is detected when *upd1* is knocked down

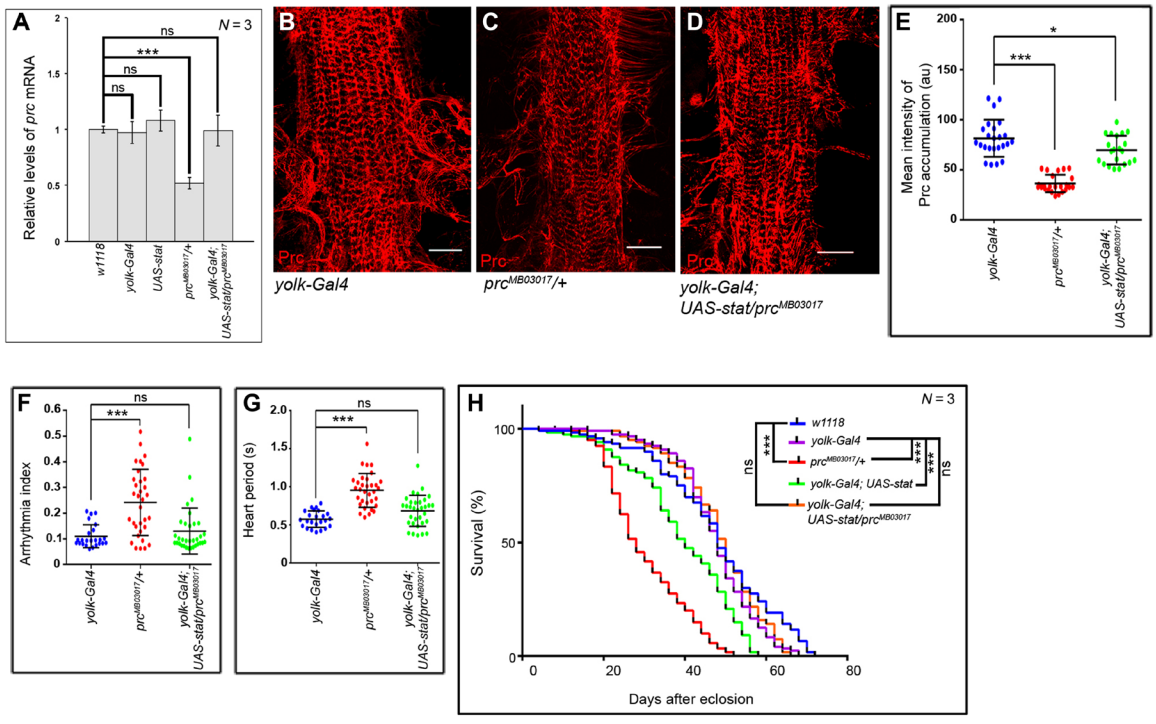

Fig. 3. Overexpression of *Stat92E* in fat cells restores the *prc* mutant phenotypes. (**A**) Rescue in *prc* expression in the fat cells of $prc^{MB03017}$/+ flies upon overexpression of *stat92E* in fat cells. The transcript levels are normalized to that of the constitutive ribosomal gene *rp49*. (**B** to **D**) Rescue in the level of Prc accumulation (red) around the second heart chamber of $prc^{MB03017}$/+ flies upon overexpression of *stat92E* in fat cells (D) as compared to that observed in $prc^{MB03017}$/+ flies (C). Prc accumulation around the second cardiac chamber of the control *yolk-Gal4* flies is shown in (B). Scale bars, 25 μm (**E**) Quantification of the mean fluorescence intensity for Prc accumulation around the second heart chamber of $prc^{MB03017}$/+ flies upon overexpression of *stat92E* in fat cells. The dots represent the samples analyzed for each genotype. (**F** and **G**) Rescue in Arrhythmia Index (F) and in Heart Period (G) of $prc^{MB03017}$/+ flies upon overexpression of *stat92E* in fat cells. The dots represent the samples analyzed for each genotype. (**H**) Overexpression of *stat92E* in the fat cells of $prc^{MB03017}$/+ flies remarkably rescues their reduced life span. While the survival rates of $prc^{MB03017}$/+ and *yolk-Gal4; UAS-stat* flies are appreciably less than that of the control w^{1118} and *yolk-Gal4* flies, the survival rate of *yolk-Gal4; UAS-stat/*$prc^{MB03017}$ flies is comparable to that of the control flies. Genotypes are as mentioned. Data are represented as means ± SD. Statistical significance with *P* values of $P < 0.05$, and $P < 0.001$ are mentioned as *, and ***, respectively.

independently in the blood cells (*hml-Gal4*), mid-gut (*esg-Gal4*), PCs (*dot-Gal4*), and muscles (*mef2-Gal4*), down-regulating *upd1* in the fat body (*yolk-Gal4*) results in a slight drop in *prc* expression (fig. S3A). On the other hand, the level of *prc* expression remains unaltered upon knocking down *upd2* in any of these tissues (fig. S3B). Likewise, knocking down *upd3* independently in the mid-gut and muscles does not lead to any drop in *prc* expression (Fig. 4B). However, a small reduction in *prc* expression is observed upon

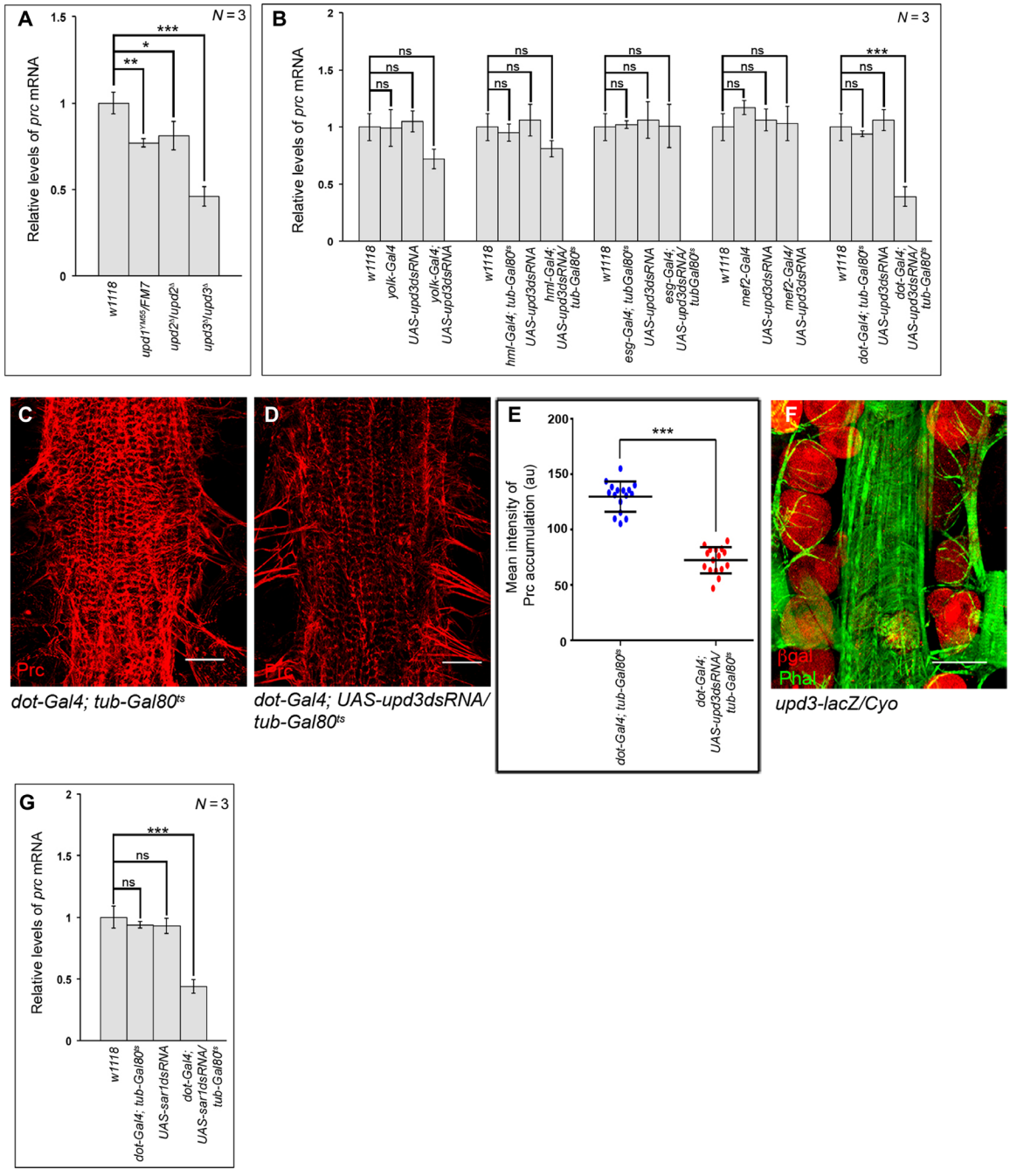

Fig. 4. Upd3 released by PCs trigger *prc* expression in the fat body cells. (**A**) Changes in *prc* expression in the fat cells of different *upd* mutants. The transcript levels are normalized to that of the constitutive ribosomal gene *rp49*. (**B**) Changes in *prc* expression in the fat cells after knocking down *upd3* from different adult tissues. The transcript levels are normalized to that of the constitutive ribosomal gene *rp49*. (**C** and **D**) Reduction in the level of Prc (red) accumulation around the second heart chamber upon knocking down *upd3* in the PCs (D) as compared to control (C). Scale bars, 25 μm. (**E**) Quantification of the mean fluorescence intensity for Prc accumulation around the second heart chamber upon knocking down *upd3* in the PCs. The dots represent the samples analyzed for each genotype. (**F**) Expression of *upd3*-lacZ (red) in the PCs. Phalloidin (green) marks the cardiac tube and the alary muscles. Scale bar, 50 μm. (**G**) Changes in the level of *prc* expression in the adult fat cells upon knocking down *sar1* in the PCs. The transcript levels are normalized to that of the constitutive ribosomal gene *rp49*. Genotypes are as mentioned. Data are represented as means ± SD. Statistical significance with *P* values of $P < 0.05$, $P < 0.01$, and $P < 0.001$ is mentioned as *, **, and ***, respectively.

knocking down *upd3* either from the fat body or from the blood cells (Fig. 4B). In contrast, knocking down *upd3* in the PCs leads to a remarkable drop in *prc* expression in the fat body (Fig. 4B) and a notable decrease in Prc accumulation around the heart (Fig. 4, C to E). In tune with these results, reporter lacZ expression for Upd3 is seen in the PCs (Fig. 4F) and preventing Upd3 release by knocking down Sar1 in the PCs results in a significant drop in *prc* expression in the fat body (Fig. 4G). The drop in *prc* expression in the fat body cells is accompanied by less deposition of Prc around the heart (fig. S3, C to E). From these results, we conclude that Upd3 from the PCs is primarily responsible for activating the JAK-STAT pathway in the fat body to trigger *prc* expression.

Upd3 expression in PCs is dependent on JNK and p38 signaling

A gamut of signaling pathways that includes Notch, TGF-β, Hippo, JNK, and p38 has been implicated to trigger the developmental expression of Upds in flies (*33*–*35*). While no detectable levels of NRE-GFP expression (Notch Response Element–GFP) (arrows in fig. S4A) are observed, nuclear expressions of Diap1-GFP (reporter for Hippo signaling) and Dad-lacZ (reporter for TGF-β signaling) are evident in the PCs (arrows in Fig. 5, A and B). Compared to these, robust expressions of TRE-DsRed (reporter for JNK signaling) (Fig. 5C) and elevated levels of phosphorylated-p38 (Fig. 5D) are detected in the PCs. To have a functional correlate of the expression studies, we systematically inactivated these pathways individually in the PCs and analyzed for *upd3* expression. Independently impairing Notch (*UAS-NdsRNA*), TGF-β (*UAS-maddsRNA*), or Hippo (*UAS-ykidsRNA*) signaling does not reduce the level of *upd3* expression (fig. S4B). However, a significant drop in *upd3* expression is detected upon attenuating either *basket* (*bsk*; codes for *Drosophila* JNK) (Fig. 5E) or *p38b* (Fig. 5F). Conversely, increased *upd3* expression in the PCs is detected upon ectopic activation of either JNKK (*hemipterous*; *hep*) (Fig. 5E) or *p38b* (Fig. 5F). In this context, it is important to note that independently down-regulating *p38a* and *p38c* in the PCs does not affect *upd3* expression (fig. S4C). A critical transcriptional effector of JNK signaling is AP1 (a heterodimer of Jun and Fos). Impairing *kayak* (*kay*; codes for *Drosophila* Fos) activity results in a marked decrease in *upd3* expression (Fig. 5E). However, knocking down of Foxo, the other transcriptional effector of JNK pathway, does not reduce *upd3* expression (fig. S4D). Besides demonstrating that both JNK and p38 signaling induce *upd3* expression in PCs, these results establish AP1 as the mediator of JNK signaling.

To delineate between JNK and p38 signaling, we analyzed the levels of phosphorylated-p38 in PCs upon inactivating JNK signaling. As evident from Fig. 5 (G to I), the levels of phosphorylated-p38 do not get affected in the PCs upon ectopic expression of bsk^{DN}. In a converse experiment, we found that knocking down *p38b* does not reduce the levels of phosphorylated-JNK in the PCs (Fig. 5, J and J′). Therefore, we conclude that combinatorial JNK and p38 signaling contribute in controlling the expression of *upd3* in PCs.

Physiological ROS regulates *upd3* expression in a JNK/p38-dependent manner

Results of our previous studies as well as from other groups have implicated high levels of ROS in developmental activation of JNK signaling in flies (*9*, *36*). Moreover, elevated levels of physiological ROS in the adult PCs triggers p38 signaling (*37*). Taking clues from these leads, we ventured to ascertain whether high levels of ROS actually induce the expression of *upd3* in the PCs. For this, we first analyzed *upd3* expression upon scavenging ROS. Overexpression of the antioxidant enzymes, Superoxide dismutase 1 (Sod1), or Catalase (Cat) leads to an appreciable drop in ROS levels (Fig. 6, A to C, and fig. S5A) and a consequent reduction in *upd3* expression (Fig. 6D). However, the levels of ROS (fig. S5, A and B) and that of *upd3* expression (Fig. 6D) remain unaltered upon overexpressing Superoxide dismutase 2 (Sod2). In concurrence, reducing the levels of Sod1 or Cat, but not Sod2, results in an increase in *upd3* expression (Fig. 6E). The drop in the levels of *upd3* expression upon scavenging the levels of ROS in the PCs eventually results in down-regulation of *prc* expression in the fat body (fig. S5C), accompanied by a reduction in Prc accumulation around the cardiac tube (fig. S5, D to G). The genetic link between elevated ROS levels and *upd3* expression in the PCs gets further endorsed as scavenging ROS affects both JNK and p38 signaling, which regulates *upd3* expression. As evident from Fig. 6 (F and G) and fig. S5H, scavenging ROS in the PCs leads to a detectable drop in the levels of phosphorylated-p38. Analogous results are observed for the expression of TRE-DsRed, the reporter for JNK signaling (Fig. 6, H and I, and fig. S5I).

Pk92B (the *Drosophila* homolog of ASK-1), which gets activated via ROS-mediated dimerization, functions as the ROS sensor in the cell (*38*). Overexpression of a dominant negative form of ASK-1, or knocking down its expression in the PCs, both lead to a drastic reduction in *upd3* expression (Fig. 7A) despite having high levels of ROS in these cells (Fig. 7, B and C, and fig. S5J). In accordance, a significant drop in the level of *prc* expression in the fat body (fig. S5K) and reduced amount of Prc accumulation in the cardiac ECM is observed (fig. S5, L to N). Furthermore, attenuating ASK-1 activity leads to a remarkable drop in both phosphorylated-p38 levels (Fig. 7, D and E, and fig. S5O) and TRE-DsRed expression (Fig. 7, F and G, and fig. S5P).

To establish the hierarchical relation between ROS and JNK or p38b, we performed genetic epistasis experiments. In one set of experiments, we analyzed the levels of *upd3* expression in PCs wherein the JNK signaling was up-regulated by expressing activated *hemipterous* (*hep*; JNKK) in a genetic background where ROS was scavenged by overexpressing Sod1. As shown in Fig. 7H, the expected drop in the level of *upd3* expression because of scavenging ROS (refer to Fig. 6D) gets rescued because of overexpression of *hep*. In another set, we analyzed the expression of *upd3* in the PCs upon knocking down *catalase* in a *p38b* dominant negative background. Attenuating p38b signaling results in suppression of the anticipated up-regulation in *upd3* expression because of elevated levels of ROS caused by down-regulation of catalase (Fig. 7H). Put together, these results demonstrate that JNK and p38b lie downstream of ROS (Fig. 7I) in regulating *upd3* expression in PCs.

NOX triggers ROS-JNK/p38 signaling to activate *upd3*

Despite the fact that both Sod1 and Sod2 are responsible for converting superoxides to peroxides, a stark difference lies in their cellular location (Fig. 8A). While Sod2 primarily scavenges superoxide radicals generated as a by-product of mitochondrial oxidative phosphorylation, cytoplasmic superoxides, mainly generated by either NAD(P)H oxidase (Nox) or dual oxidase (Duox) activity, are scavenged by Sod1 (*4*). Given that the levels of ROS in the PCs can be modulated by genetically altering the expression of Sod1, but not Sod2 (refer to Fig. 6, A and B, and fig. S5B), we conjectured that increased activity of Nox or Duox might contribute to the physiological ROS

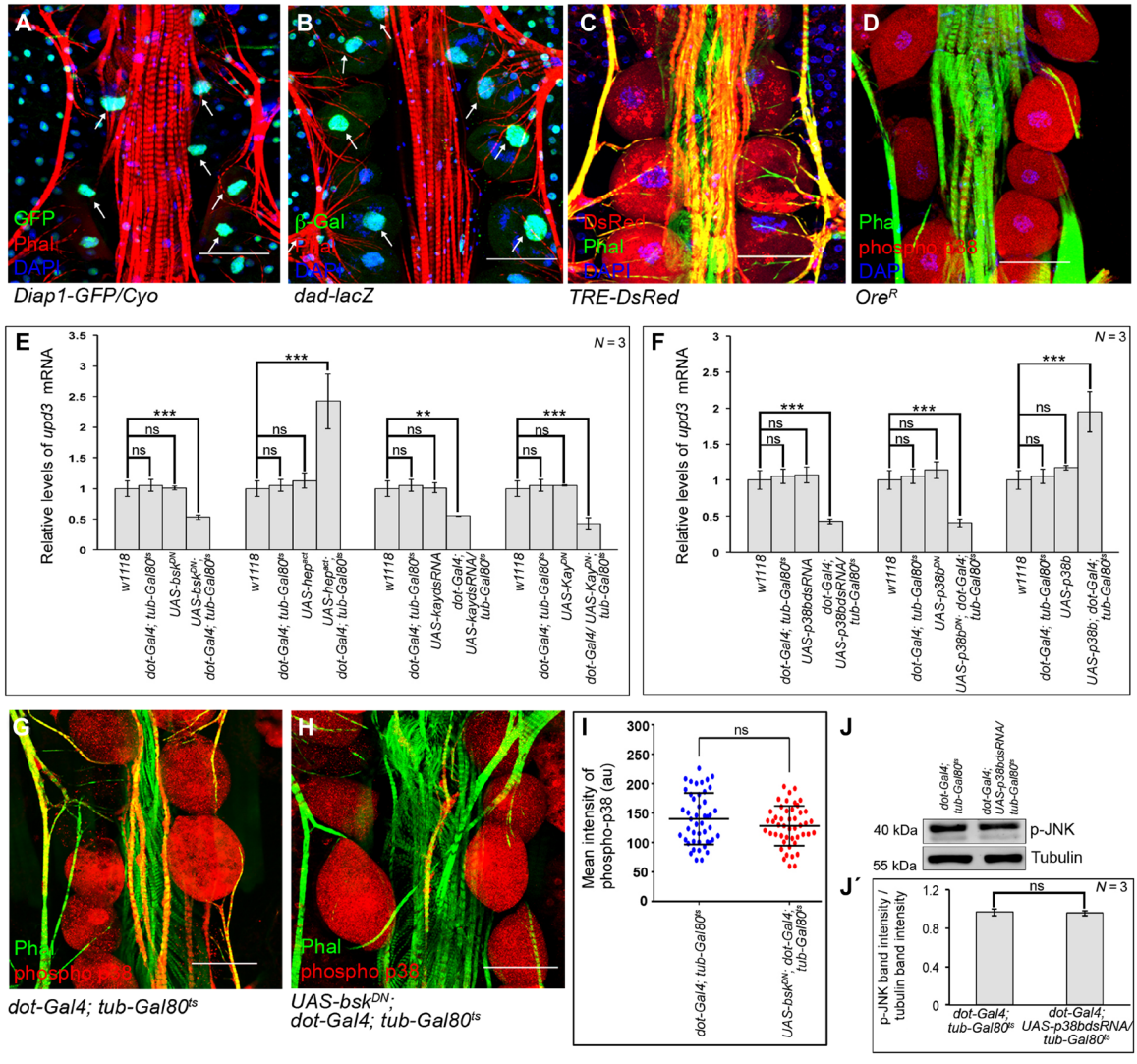

Fig. 5. JNK and p38 signaling activates *upd3* in the PCs. (**A** and **B**) Expressions of *Diap1-GFP* (green; Hippo pathway) (A) and that of *dad-lacZ* (green; Dpp signaling) (B) in the PCs. Phalloidin (red) marks the cardiac tube and the alary muscles. DAPI (blue) marks the nuclei. Arrows refer to the nuclei of PCs. (**C** and **D**) Expression of *TRE-DsRed* (red; JNK pathway) (C) and the levels of phosphorylated-p38 (red) (D) in the PCs. Phalloidin (green) marks the cardiac tube and the alary muscles. DAPI (blue) marks the nuclei. (**E** and **F**) Changes in the expression of *upd3* upon modulating JNK signaling (E) or p38b signaling (F) in the PCs. The transcript levels are normalized to that of the constitutive ribosomal gene *rp49*. (**G** and **H**) Levels of phosphorylated-p38 (red) in the PCs upon inactivating JNK signaling (H) as compared to control (G). Phalloidin (green) marks the cardiac tube and the alary muscles. (**I**) Quantification of the mean fluorescence intensity for phosphorylated-p38 level in the PCs. The dots represent the number of PCs analyzed for each genotype. (**J** and **J´**) Immunoblot analyses demonstrating the unchanged level of phosphorylated JNK upon down-regulating *p38b* in the PCs. Tubulin serves as the loading control (J). Quantification of the phosphorylated JNK band intensities normalized to that of Tubulin band intensities (J´). Genotypes are as mentioned. Scale bars, 50 μm in all images. Data are represented as means ± SD. Statistical significance with *P* values of $P < 0.01$, and $P < 0.001$ are mentioned as **, and ***, respectively.

in the PCs. Indeed, down-regulating Nox activity results in a marked decrease in ROS levels (Fig. 8, B and C, and fig. S6A). The ROS levels upon knocking down Duox, however, remain unaltered when compared to control (Fig. 8D and fig. S6A). Accordingly, a notable drop in *upd3* expression is observed upon knocking down *nox*, while the level of *upd3* expression remains unaltered upon knocking down *duox* (Fig. 8E). In summary, these results put Nox activity as the major source for high levels of ROS that controls *upd3* expression in the PCs.

That Nox regulates the expression of *upd3* involving the ROS-JNK/p38 axis gets further established as specifically knocking down *nox* in the PCs results in an appreciable drop in the expression of TRE-DsRed (Fig. 8, F and G, and fig. S6B) and in the levels of phosphorylated-p38 (Fig. 8, H and I, and fig. S6C) in these cells. Last, we checked for the levels of *prc* expression in the fat body of flies with *nox* being inactivated in the PCs. As evident from Fig. 8J, down-regulating *nox* in the PCs results in a significant drop in *prc* expression in fat cells. A notable reduction in Prc accumulation around the cardiac tube (fig. S6, D to F) is also observed. From all these results, we conclude that the Nox-ROS-Ask1-JNK/p38 signaling cascade is instrumental in regulating *upd3* expression in the PCs.

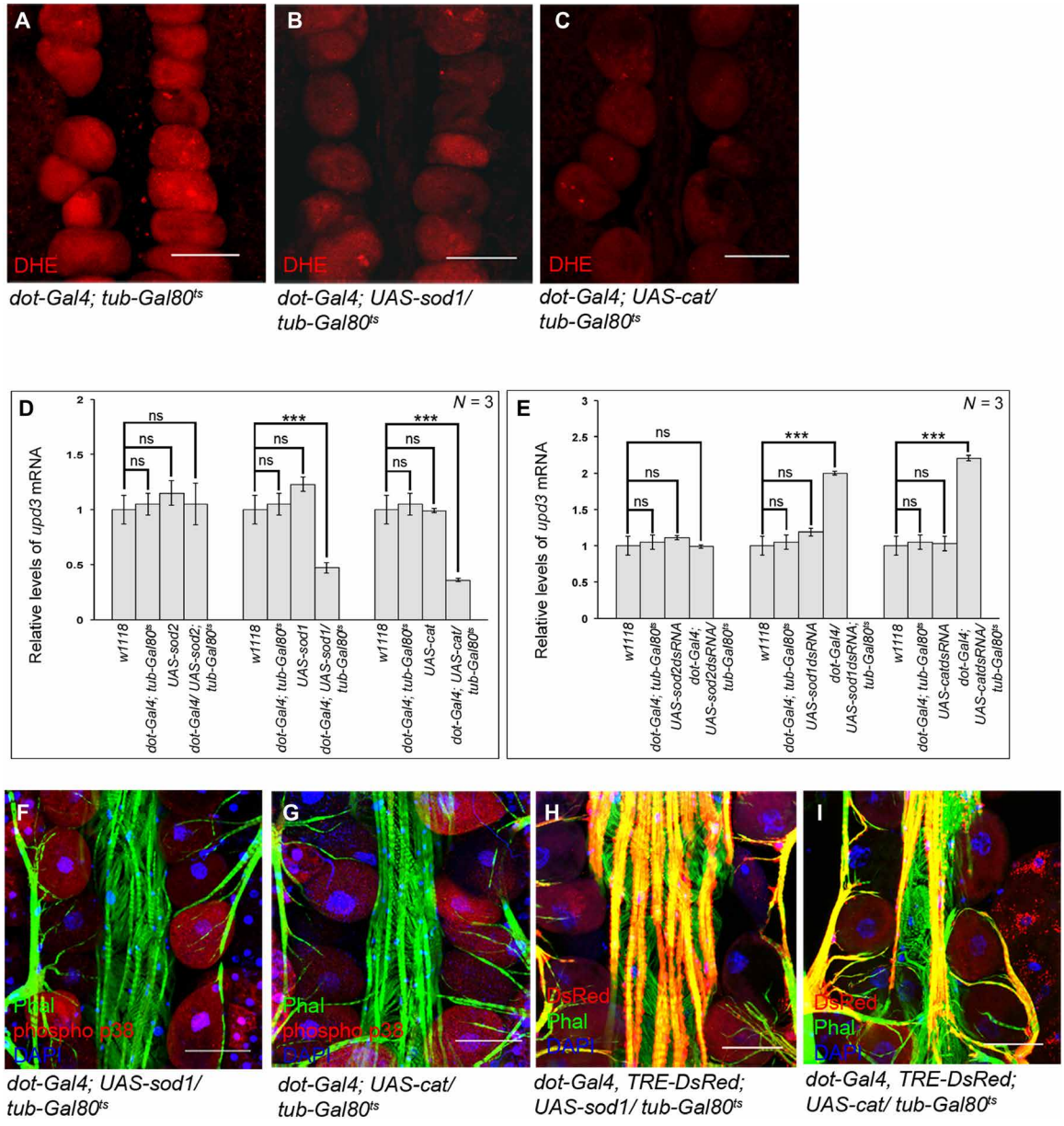

Fig. 6. ROS-dependent activation of p38 and JNK signaling in the PCs. (**A** to **C**) Drop in the levels of ROS (DHE staining; red) in the PCs upon overexpression of SOD1 (B) or Catalase (C) as compared to control (A). (**D**) Changes in *upd3* expression upon overexpression of SOD2, SOD1, and Catalase in the PCs. The transcript levels are normalized to that of the constitutive ribosomal gene *rp49*. (**E**) Changes in *upd3* expression upon down-regulating the levels of SOD2, SOD1, and Catalase in the PCs. The transcript levels are normalized to that of the constitutive ribosomal gene *rp49*. (**F** and **G**) Reduction in the levels of phosphorylated-p38 (red) in the PCs upon scavenging ROS by overexpression of SOD1 (F) or Catalase (G). Phalloidin (green) marks the cardiac tube and the alary muscles. DAPI (blue) marks the nuclei. (**H** and **I**) Drop in *TRE-DsRed* expression (red) in the PCs upon scavenging ROS by overexpression of SOD1 (H) or Catalase (I). Phalloidin (green) marks the cardiac tube and the alary muscles. DAPI (blue) marks the nuclei. Genotypes are as mentioned. Scale bars, 50 μm in all images. Data are represented as means ± SD. Statistical significance with *P* values of $P < 0.001$ is mentioned as ***.

DISCUSSION

Our in vivo molecular and genetic analyses provide direct evidence linking the physiological ROS level of the PCs in regulating the fat cell–specific expression of *prc*, essential for modeling cardiac ECM in *Drosophila*. This feat is primarily achieved by regulating the expression of the cytokine Upd3 in the PCs (Fig. 8K). Our genetic analyses show that the physiological ROS level induces the expression of *upd3* in PCs by activating the well-conserved ASK1-JNK/p38 signaling axis. In turn, Upd3 released by the PCs triggers JAK-STAT signaling responsible for *prc* expression in the fat cells. Alteration of the ROS level or genetic manipulation of any member of the signaling cascade leads to the loss of this control. The inter-organ communication identified in this study is physiologically relevant as incorporating the optimal amount of Prc in the cardiac ECM of otherwise normal adult flies is critical for routine cardiac function and a healthy life span. Our results, therefore, shed light on

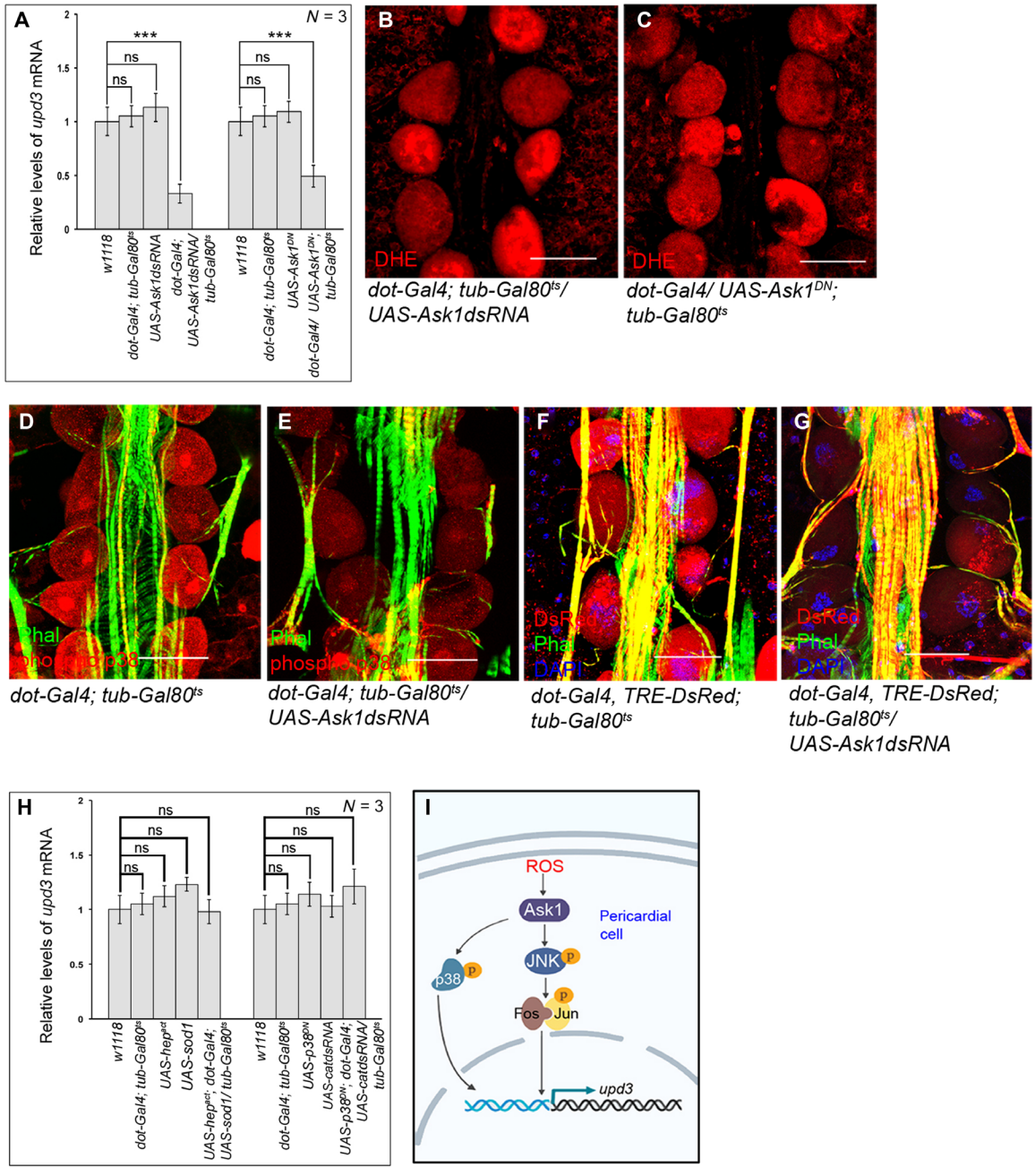

Fig. 7. Ask1 links ROS to JNK and p38 signaling pathways. (**A**) Reduction in *upd3* expression in the PCs upon down-regulating Ask1 activity. The transcript levels are normalized to that of the constitutive ribosomal gene *rp49*. (**B** and **C**) Levels of ROS (DHE staining; red) in the PCs remain unchanged upon down-regulating Ask1 activity. (**D** and **E**) Drop in the levels of phosphorylated-p38 (red) in the PCs upon down-regulating *Ask1* (E) as compared to control (D). Phalloidin (green) marks the cardiac tube and the alary muscles. (**F** and **G**) Reduction in *TRE-DsRed* expression (red) in the PCs upon down-regulating *Ask1* (G) as compared to control (F). Phalloidin (green) marks the cardiac tube and the alary muscles. DAPI (blue) marks the nuclei. (**H**) Levels of *upd3* expression in the PCs of the flies of the mentioned genotypes. The transcript levels are normalized to that of the constitutive ribosomal gene *rp49*. (**I**) Signaling cascade triggered by ROS to regulate *upd3* expression in the PCs. Genotypes are as mentioned. Scale bars, 50 μm in all images. Data are represented as means ± SD. Statistical significance with *P* values of $P < 0.001$ is mentioned as ***.

an unexpected role of ROS as a metabolic signal essential for supporting cardiac function by modeling the cardiac ECM.

Studies in the recent past have identified physiological ROS as a metabolic signal to regulate fundamental cell biological processes (*4*, *39*). While, in most cases, the manifestation of ROS-mediated physiological and pathological responses occur because of cell-autonomous activation of specific signaling pathways by ROS, a growing body of reports advocates for the paracrine role of ROS. For instance, wound-derived H_2O_2 diffuses into the neighboring neutrophils to direct their recruitment to the wound site (*40*, *41*), release

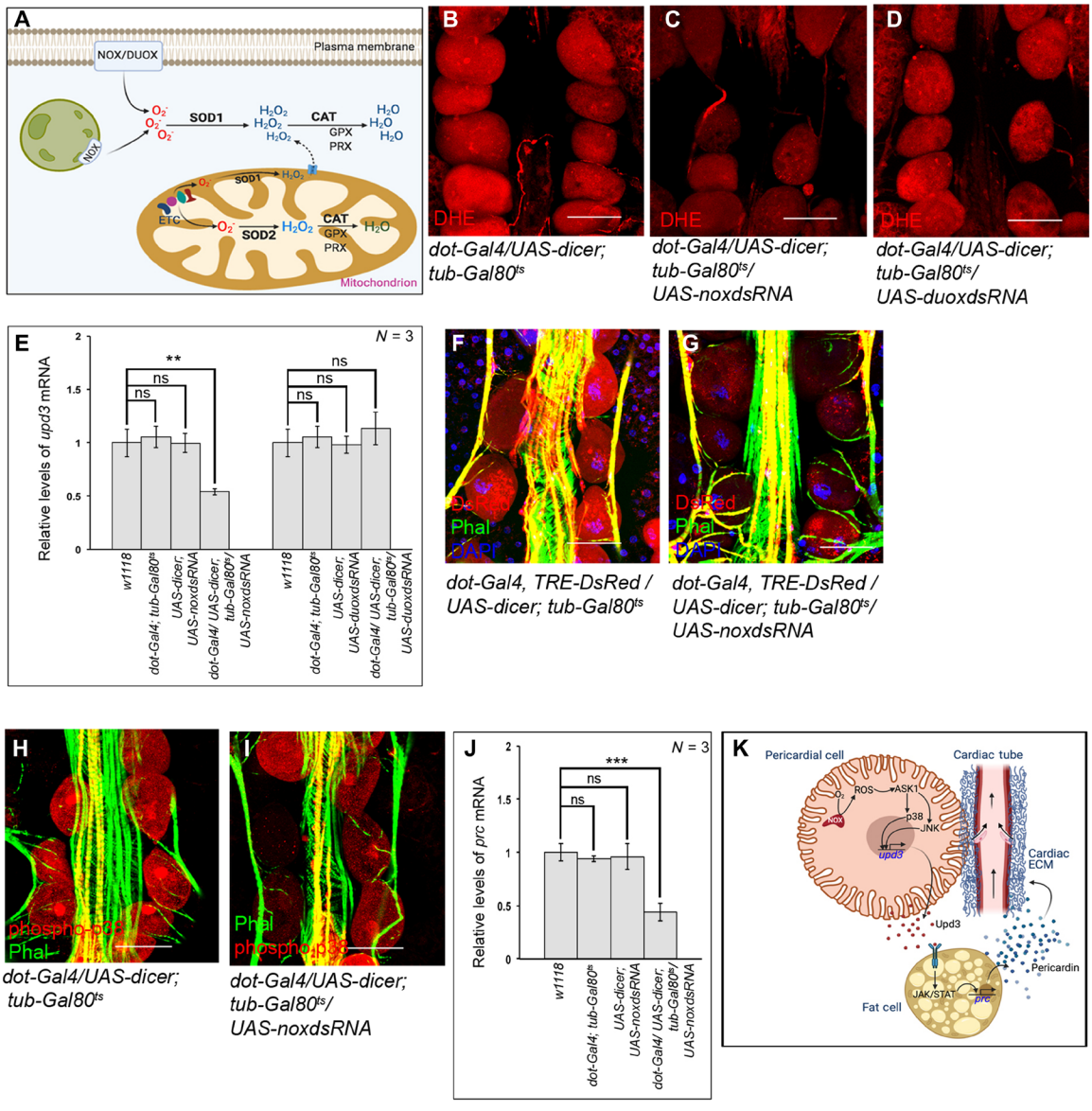

Fig. 8. Nox activity generates physiological levels of ROS in the PCs. (**A**) Schematic representation demonstrating the redox homeostasis between generating and scavenging of ROS within a cell. (**B** to **D**) Changes in the levels of ROS (DHE staining; red) in the PCs upon knocking down *nox* (C) and *duox* (D) as compared to control (B). (**E**) Changes in *upd3* expression upon independently down-regulating *nox* and *duox* in the PCs. The transcript levels are normalized to that of the constitutive ribosomal gene *rp49*. (**F** and **G**) Reduction in *TRE-DsRed* expression (red) in the PCs upon knocking down *nox* (G) as compared to control (F). Phalloidin (green) marks the cardiac tube and the alary muscles. DAPI (blue) marks the nuclei. (**H** and **I**) Drop in the levels of phosphorylated-p38 (red) in the PCs upon knocking down *nox* (I) as compared to control (H). Phalloidin (green) marks the cardiac tube and the alary muscles. (**J**) Alteration in the level of *prc* expression in fat cells after knocking down *nox* in the PCs. The transcript levels are normalized to that of the constitutive ribosomal gene *rp49*. (**K**) Model showing the inter-organ communication circuitry connecting PCs and fat cells to regulate cardiac function by controlling Prc deposition in the cardiac ECM of adult flies. Arrows in the cardiac tube mark the directionality of hemolymph flow. Genotypes are as mentioned. Scale bars, 50 μm in all images. Data are represented as means ± SD. Statistical significance with *P* values of $P < 0.01$, and $P < 0.001$ are mentioned as **, and ***, respectively.

of ROS and extracellular vesicles containing ROS-generating membrane protein complexes by neutrophils and macrophages signal the injured axons to regenerate (*42*), and in vitro treatment of neonatal mouse cardiomyocytes with a low level of ROS stimulates proliferation (*43*). Likewise, ROS generated by the dying cells propagate to the nearby surviving cells to drive multiple functions associated with tissue repair and regeneration in the larval imaginal discs of *Drosophila* (*35*). From that perspective, our findings shed light on another interesting mechanism by which physiological ROS could impart its paracrine role. Rather than being released out, ROS activates a signaling cascade that regulates the expression of a cytokine, Upd3, that functions as a paracrine signaling molecule. While the previously identified paracrine roles of ROS are relatively local in nature, the one identified here imparts trans-organ effects. Considering

the pleiotropic nature of cytokines, this kind of regulation seems more systemic as it has the potential to modulate multiple processes in diverse tissues.

The nonmyocytic PCs, flanking the cardiac tube, primarily function as nephroctyes to filter proteins and toxic molecules from the hemolymph that are targeted for either lysosome-mediated degradation or are recycled back to the hemolymph (*44*, *45*). Our study unravels the mechanistic basis of a metabolic role of the PCs, quite distinct from their normal nephrocytic function, in regulating cardiac activity in *Drosophila*. Studies in the recent past identified that elevated levels of pericardial ROS, in a p38-dependent manner, regulates the function of the neighboring cardiomyocytes involving two septate junction proteins, Cora and Kune (*46*). However, the underlying mechanism remains elusive. Compared to this kind of modulation of local interaction between the two neighboring cells, the mechanism identified in this study evidences a more influential role of pericardial ROS in regulating cardiac function. Given the overarching role of ECM in regulating cell structure and signaling (*47*), it is intuitively apparent that modulation of the cardiac ECM composition would have a more encompassing impact on the functioning of the heart. One possible aspect might be the requirement of an optimal amount of Prc in the cardiac ECM to regulate the proper interaction between the Kune proteins of the PCs and the cardiomyocytes. While an increase in Prc level by supraphysiological levels of pericardial ROS may reduce interaction between the Kune proteins of the PCs and the cardiomyocytes, the reverse can be true for subphysiological levels of pericardial ROS. Irrespective of the mechanism involved, and given that (i) the PCs constitute a vital component of the fly renal system (*48*) and function as the primary filtration unit for hemolymph, and (ii) pumping of the cardiac tube controls the flow of hemolymph, regulation of cardiac function by PCs indicates a physiological process critical for systemic homeostasis. It probably coordinates the rate of movement of hemolymph within the body with the PCs' filtration capacity. In a sense, this appears to be a rudimentary and evolutionarily primitive version of the heart-kidney link observed in higher vertebrates.

Another fascinating outcome of this study is the role of Upd3 in modulating the expression of *prc* in fat cells. Like many mammalian cytokines, Upd3 plays a vital role in *Drosophila* immune response. While *upd3* is transcriptionally activated in the adult fat bodies in response to septic injury (*49*), upon wasp infestation, larval hemocytes release Upd3 to activate JAK/STAT signaling in the muscles to launch an efficient cellular response (*50*). In addition, Upd3 is also involved in stem cell homeostasis (*29*, *51*), regulating cardiomyocyte function (*52*), and generating insulin resistivity in response to high dietary fat (*53*). Here, we identify a physiological requirement for Upd3 released from the PCs in collagen synthesis and ECM remodeling. The impact of Upd3 released from other possible adult tissues on *prc* expression is not that prominent. Although the reason behind distinct roles played by Upd3 released from different sources remains to be determined, it would be equally important to determine whether Upd3 produced by the PCs can target tissues beyond the fat cells. In this context, it is important to note that several animal models of fibrosis, a pathological condition associated with excessive collagen accumulation, have documented the controversial roles of cytokines in regulating collagen synthesis (*54*, *55*). While some cytokines have profibrotic functions (*56*, *57*), others can act as antifibrotic agents (*58*, *59*). However, the pleiotropic activities of cytokines, differences between acute and chronic actions, and the large number of cytokines coded by the mammalian genome make it challenging to unravel the mechanism involved in cytokine-dependent regulation of collagen synthesis essential for ECM modeling during normal development. Future work will be of interest to examine the involvement of the mechanism identified here in cytokine-dependent collagen synthesis in mammals during normal physiological conditions as well as during fibrosis.

In conclusion, the present work unravels the molecular genetic basis of a fascinating example of an inter-organ cross-talk triggered by ROS. Identification of this physiologically relevant communication network not only connects the metabolic state of a vital peripheral organ in regulating the flow of blood/hemolymph but also provides evidence for a previously unrecognized paracrine role of physiological ROS in cytokine-dependent ECM modeling with implications in fibrosis and other pathophysiological conditions.

MATERIALS AND METHODS

Drosophila stocks and fly husbandry

All the fly stocks were routinely maintained at 25°C (if not otherwise mentioned) on a standard cornmeal-agar food. Twenty-day-old adult female flies were used for all the analyses. To induce transgene expression using GAL4 drivers, flies were maintained at 18°C till eclosion. Two-day-old freshly eclosed flies were reared at 29°C for 14 days (equivalent to 18 days at 25°C) for analyses. The list of fly strains used is provided in table S1.

Immunostaining of adult cardiac tissue and PCs

All immunostaining experiments were performed at least thrice following the standard protocol. Adult female abdomens were dissected on ice in 1× phosphate-buffered saline (PBS), fixed in 6% paraformaldehyde for 2 hours at room temperature (RT), and washed with 0.3% PBT (0.3% TritonX100 in 1XPBS) for 90 min. Then, tissues were incubated in primary antibody diluted in PAXDG (0.3% PBT with 0.3% sodium deoxycholate, 5% normal goat serum, and 1% bovine serum albumin) at 4°C for 24 hours. Following washes in 0.3% PBT, incubation in secondary antibody in PAXDG was done at 4°C for 24 hours. The tissues were washed in PBT and stained with phalloidin (1:500 in PBS) at 4°C for 48 hours followed by staining with 4′,6-diamidino-2-phenylindole at RT for 30 min. For all samples processed in parallel, immunofluorescence images were captured in a Leica SP8 confocal microscope under identical conditions (laser power, gain, and scan settings) and analyzed and processed under the same conditions using Fiji software. The following primary antibodies were used: mouse anti-Prc (1:10; DSHB EC11), rabbit anti-phospho p38 (1:100; Thr^{180}/Tyr^{182}, clone 3D7; Cell Signaling Technology), and mouse anti-β galactosidase (1:100; Promega no. Z3781).

Detection of ROS

ROS detection with DHE dye (Molecular Probes no. D11347, Invitrogen) was performed as published earlier (*60*). Briefly, the adult female abdomens were dissected in 1× PBS followed by incubation in 30 μM DHE Solution for 15 min at RT under dark conditions. Tissues were then washed with 1× PBS, fixed in 10% paraformaldehyde for 10 min, and then washed with 1× PBS for 5 min. The samples processed in parallel were mounted and immediately imaged using a Leica SP8 confocal microscope under identical conditions (laser power, gain, and frame size) and analyzed and processed under the same conditions using Fiji software.

RNA isolation from adult cardiac tissue and fat body

Adult cardiac tubes or fat body cells from around 40 to 50 female flies were dissected in 1× PBS. Isolation of RNA was performed by TRIzol (Ambion no. 15596018) following the manufacturer's instructions. cDNA was produced using Verso cDNA synthesis kit (Molecular Probes no. AB1453A) following the manufacturer's recommended protocol. Real-time quantitative polymerase chain reaction (RT-qPCR) was conducted using the TB Green Premix Ex Taq TM (Tli RNaseH Plus) (Takara no. RR440A) on the Bio-Rad CFX96 Touch Real-Time PCR Detection System. To determine the optimal Tm for each primer set, graded RT-qPCR was performed. The relative levels of mRNAs were determined using the $2^{-\Delta Ct}$ method. The transcript levels were normalized to the constitutive ribosomal gene coding for ribosomal protein 49 (rp49) transcript levels. RT-qPCR experiments were conducted on three to four independent cDNA samples per condition. The figures represent the combined data from all samples. Primers were so designed that they span the exon-exon junction. A list of primers used in our RT-qPCR experiments is available in table S2.

Protein isolation and Western blotting from whole abdomen and adult cardiac tissue of *Drosophila*

For protein isolation, around 15 to 20 cardiac tubes were homogenized in 1% Triton X-100 in 1× PBS buffer (pH 7.2) supplemented with 1% mammalian Protease Inhibitor Cocktail (Sigma-Aldrich, P8340) on ice. The homogenate was centrifuged at 20,000*g* for 15 min at 4°C. The supernatant was mixed with equal volume of 2× Laemmli Buffer [100 mM tris-HCl (pH 6.8); 4% SDS: Sigma-Aldrich, catalog no. L3771; 0.2% Bromophenol Blue, HIMEDIA, catalog no. MB123; 20% glycerol and 200 mM b-mercaptoethanol, Sigma-Aldrich, catalog no. M3148], boiled at 95°C for 5 min, and used. The protein quantitation was done using Bradford Assay (Bio-Rad, catalog no. 5000006). One microliter of protein sample was incubated in 1 ml of five times diluted Bradford reagent, incubated for 5 min at RT, and the OD of the mix was measured at 595 nm in a spectrophotometer. The concentration of protein was calculated using a standard curve prepared freshly. For Western blot analyses of Prc, the samples were homogenized in ECM extraction buffer (mix 2 mM EDTA with 4 M urea in 1:1 ratio and add 1.5% Triton X-100). The rest of the protocol followed is the same as mentioned above. The primary antibodies used for Western blot analysis are as follows: mouse anti-Tubulin (1:1000; Sigma-Aldrich, T6199), rabbit anti-active pJNK (1:1000; Promega, no. V7931), and mouse anti-Prc (1:100; DSHB no. EC11). Horseradish peroxidase (HRP)–conjugated anti-mouse (GenScript, no. A00160) and HRP-conjugated anti rabbit (GenScript, no. A00098) at 1:5000 dilution were used as the secondary antibodies. Blots were developed using Luminata Crescendo Western HRP substrate (Millipore). The band intensities were analyzed using ImageJ and normalized with tubulin bands that served as loading controls. Western blot analyses were conducted on three to four independent protein samples per condition. The graphs represent the combined data from all samples.

Fly heartbeat analysis

Semi-intact female *Drosophila* was used for measuring the cardiac contractility as described previously (*61*). High-speed digital movies of beating hearts were captured using QImaging optiMOS scMOS camera R-M-16-C at 100 fps for 10 s with a 20× water immersion lens (Zeiss). M-modes and quantitative data were generated using SOHA, a MATLAB-based image analysis software (*61*).

Life-span analysis

All the life-span experiments were performed independently using three to four replicates of 60 flies each (40 females and 20 males) per genotype. The flies were transferred to fresh food bottles every day. Dead female flies in each bottle were counted and removed when the flies were flipped. The survival curves of the females for each genotype (n = 120 to 160 flies, from three to four independent replicates) were generated in GraphPad Prism version 6.00 (La Jolla, CA) using a log-rank Mantel-Cox test.

Intensity analysis of images

For intensity analyses of DHE, phospho-p38, and TRE-dsRed, the PCs of the control and experimental samples were marked, and the mean fluorescence intensity (mean gray value) was measured using Fiji software. To determine the intensity of Prc accumulation around the second chamber of the cardiac tube, the entire second chamber was marked and the mean fluorescence intensity (mean gray value) was measured using Fiji software. For the samples processed in parallel, all the analyses were done under identical conditions. From these readings, the average mean gray values (for the same size of region of interest) of the background were deducted to obtain the mean gray value minus blank. The intensity values were plotted using GraphPad Prism version 6.00 (La Jolla, CA) where the dots represent the number of samples analyzed, and the error bars represent SD.

Quantification and statistical analysis

Statistical analyses of the data were performed by using either unpaired Student's t test (two-tailed) with Welch's correction or one-way analysis of variance (ANOVA) followed by Bonferroni correction using GraphPad Prism 6 software. Kaplan-Meier survival curves were generated with GraphPad Prism 6 software and curve comparison was done using Log-Rank (Mantel-Cox) test for the life-span data. All the plotted survival graphs represent the combined data of three to four independent repeats of 40 flies per genotype. Statistical significance was accepted with P values of <0.05; <0.01; and <0.001, mentioned as *, **, and ***, respectively.

SUPPLEMENTARY MATERIALS

Supplementary material for this article is available at https://science.org/doi/10.1126/sciadv.abj4991

View/request a protocol for this paper from *Bio-protocol*.

REFERENCES AND NOTES

1. A. Glasauer, N. S. Chandel, ROS. *Curr. Biol.* **23**, R100–R102 (2013).
2. C. L. Quinlan, I. V. Perevoshchikova, M. Hey-Mogensen, A. L. Orr, M. D. Brand, Sites of reactive oxygen species generation by mitochondria oxidizing different substrates. *Redox Biol.* **1**, 304–312 (2013).
3. W. Droge, Free radicals in the physiological control of cell function. *Physiol. Rev.* **82**, 47–95 (2002).
4. M. Schieber, N. S. Chandel, ROS function in redox signaling and oxidative stress. *Curr. Biol.* **24**, R453–R462 (2014).
5. T. Kietzmann, A. Gorlach, Reactive oxygen species in the control of hypoxia-inducible factor-mediated gene expression. *Semin. Cell Dev. Biol.* **16**, 474–486 (2005).
6. M. D. Buck, R. T. Sowell, S. M. Kaech, E. L. Pearce, Metabolic instruction of immunity. *Cell* **169**, 570–586 (2017).
7. T. F. Beckhauser, J. Francis-Oliveira, R. De Pasquale, Reactive oxygen species: Physiological and physiopathological effects on synaptic plasticity. *J. Exp. Neurosci.* **10**, 23–48 (2016).
8. Y. Higashi, S. Sasaki, K. Nakagawa, H. Matsuura, T. Oshima, K. Chayama, Endothelial function and oxidative stress in renovascular hypertension. *N. Engl. J. Med.* **346**, 1954–1962 (2002).
9. A. G. Toshniwal, S. Gupta, L. Mandal, S. Mandal, ROS inhibits cell growth by regulating 4EBP and S6K, independent of TOR, during development. *Dev. Cell* **49**, 473–489.e9 (2019).

10. A. Nugud, D. Sandeep, A. T. El-Serafi, Two faces of the coin: Minireview for dissecting the role of reactive oxygen species in stem cell potency and lineage commitment. *J. Adv. Res.* **14**, 73–79 (2018).
11. C. Dunnill, T. Patton, J. Brennan, J. Barrett, M. Dryden, J. Cooke, D. Leaper, N. T. Georgopoulos, Reactive oxygen species (ROS) and wound healing: The functional role of ROS and emerging ROS-modulating technologies for augmentation of the healing process. *Int. Wound J.* **14**, 89–96 (2017).
12. T. Finkel, The metabolic regulation of aging. *Nat. Med.* **21**, 1416–1423 (2015).
13. H. Huang, W. Du, R. A. Brekken, Extracellular matrix induction of intracellular reactive oxygen species. *Antioxid. Redox Signal.* **27**, 774–784 (2017).
14. E. Werner, Z. Werb, Integrins engage mitochondrial function for signal transduction by a mechanism dependent on Rho GTPases. *J. Cell Biol.* **158**, 357–368 (2002).
15. S. Honore, H. Kovacic, V. Pichard, C. Briand, J. B. Rognoni, Alpha2beta1-integrin signaling by itself controls G1/S transition in a human adenocarcinoma cell line (Caco-2): Implication of NADPH oxidase-dependent production of ROS. *Exp. Cell Res.* **285**, 59–71 (2003).
16. W. Sangrar, Y. Gao, M. Scott, P. Truesdell, P. A. Greer, Fer-mediated cortactin phosphorylation is associated with efficient fibroblast migration and is dependent on reactive oxygen species generation during integrin-mediated cell adhesion. *Mol. Cell. Biol.* **27**, 6140–6152 (2007).
17. K. Mori, T. Uchida, T. Yoshie, Y. Mizote, F. Ishikawa, M. Katsuyama, M. Shibanuma, A mitochondrial ROS pathway controls matrix metalloproteinase 9 levels and invasive properties in RAS-activated cancer cells. *FEBS J.* **286**, 459–478 (2019).
18. V. M. Chen, P. J. Hogg, Allosteric disulfide bonds in thrombosis and thrombolysis. *J. Thromb. Haemost.* **4**, 2533–2541 (2006).
19. S. Kaewpila, S. Venkataraman, G. R. Buettner, L. W. Oberley, Manganese superoxide dismutase modulates hypoxia-inducible factor-1 alpha induction via superoxide. *Cancer Res.* **68**, 2781–2788 (2008).
20. J. Myllyharju, E. Schipani, Extracellular matrix genes as hypoxia-inducible targets. *Cell Tissue Res.* **339**, 19–29 (2010).
21. N. Sampson, P. Berger, C. Zenzmaier, Redox signaling as a therapeutic target to inhibit myofibroblast activation in degenerative fibrotic disease. *Biomed. Res. Int.* **2014**, 131737 (2014).
22. J. L. Barnes, Y. Gorin, Myofibroblast differentiation during fibrosis: Role of NAD(P)H oxidases. *Kidney Int.* **79**, 944–956 (2011).
23. B. Rotstein, A. Paululat, On the morphology of the *Drosophila* heart. *J. Cardiovasc. Dev. Dis.* **3**, 15 (2016).
24. A. Chartier, S. Zaffran, M. Astier, M. Semeriva, D. Gratecos, Pericardin, a Drosophila type IV collagen-like protein is involved in the morphogenesis and maintenance of the heart epithelium during dorsal ectoderm closure. *Development* **129**, 3241–3253 (2002).
25. M. Drechsler, A. C. Schmidt, H. Meyer, A. Paululat, The conserved ADAMTS-like protein lonely heart mediates matrix formation and cardiac tissue integrity. *PLOS Genet.* **9**, e1003616 (2013).
26. A. C. Wilmes, N. Klinke, B. Rotstein, H. Meyer, A. Paululat, Biosynthesis and assembly of the Collagen IV-like protein Pericardin in *Drosophila melanogaster*. *Biol. Open* **7**, bio030361 (2018).
27. J. S. Bonifacino, B. S. Glick, The mechanisms of vesicle budding and fusion. *Cell* **116**, 153–166 (2004).
28. S. X. Hou, Z. Zheng, X. Chen, N. Perrimon, The Jak/STAT pathway in model organisms: Emerging roles in cell movement. *Dev. Cell* **3**, 765–778 (2002).
29. M. Amoyel, E. A. Bach, Functions of the Drosophila JAK-STAT pathway: Lessons from stem cells. *JAKSTAT* **1**, 176–183 (2012).
30. E. A. Bach, L. A. Ekas, A. Ayala-Camargo, M. S. Flaherty, H. Lee, N. Perrimon, G. H. Baeg, GFP reporters detect the activation of the Drosophila JAK/STAT pathway in vivo. *Gene Expr. Patterns* **7**, 323–331 (2007).
31. D. F. Eberl, L. A. Perkins, M. Engelstein, A. J. Hilliker, N. Perrimon, Genetic and developmental analysis of polytene section 17 of the X chromosome of *Drosophila melanogaster*. *Genetics* **130**, 569–583 (1992).
32. D. Osman, N. Buchon, S. Chakrabarti, Y. T. Huang, W. C. Su, M. Poidevin, Y. C. Tsai, B. Lemaitre, Autocrine and paracrine unpaired signaling regulate intestinal stem cell maintenance and division. *J. Cell Sci.* **125**, 5944–5949 (2012).
33. J. L. Chao, Y. C. Tsai, S. J. Chiu, Y. H. Sun, Localized Notch signal acts through eyg and upd to promote global growth in Drosophila eye. *Development* **131**, 3839–3847 (2004).
34. P. Houtz, A. Bonfini, X. Liu, J. Revah, A. Guillou, M. Poidevin, K. Hens, H. Y. Huang, B. Deplancke, Y. C. Tsai, N. Buchon, Hippo, TGF-β, and Src-MAPK pathways regulate transcription of the *upd3* cytokine in *Drosophila* enterocytes upon bacterial infection. *PLOS Genet.* **13**, e1007091 (2017).
35. P. Santabarbara-Ruiz, P. Santabárbara-Ruiz, M. López-Santillán, I. Martínez-Rodríguez, A. Binagui-Casas, L. Pérez, M. Milán, M. Corominas, F. Serras, ROS-induced JNK and p38 signaling is required for unpaired cytokine activation during *Drosophila* regeneration. *PLOS Genet.* **11**, e1005595 (2015).
36. E. Owusu-Ansah, A. Yavari, S. Mandal, U. Banerjee, Distinct mitochondrial retrograde signals control the G1-S cell cycle checkpoint. *Nat. Genet.* **40**, 356–361 (2008).
37. H. Y. Lim, W. Wang, J. Chen, K. Ocorr, R. Bodmer, ROS regulate cardiac function via a distinct paracrine mechanism. *Cell Rep.* **7**, 35–44 (2014).
38. Y. Sekine, R. Hatanaka, T. Watanabe, N. Sono, S. I. Iemura, T. Natsume, E. Kuranaga, M. Miura, K. Takeda, H. Ichijo, The Kelch repeat protein KLHDC10 regulates oxidative stress-induced ASK1 activation by suppressing PP5. *Mol. Cell* **48**, 692–704 (2012).
39. P. D. Ray, B. W. Huang, Y. Tsuji, Reactive oxygen species (ROS) homeostasis and redox regulation in cellular signaling. *Cell. Signal.* **24**, 981–990 (2012).
40. P. Niethammer, C. Grabher, A. T. Look, T. J. Mitchison, A tissue-scale gradient of hydrogen peroxide mediates rapid wound detection in zebrafish. *Nature* **459**, 996–999 (2009).
41. S. K. Yoo, T. W. Starnes, Q. Deng, A. Huttenlocher, Lyn is a redox sensor that mediates leukocyte wound attraction in vivo. *Nature* **480**, 109–112 (2011).
42. A. Hervera, F. de Virgiliis, I. Palmisano, L. Zhou, E. Tantardini, G. Kong, T. Hutson, M. C. Danzi, R. B. T. Perry, C. X. C. Santos, A. N. Kapustin, R. A. Fleck, J. A. del Río, T. Carroll, V. Lemmon, J. L. Bixby, A. M. Shah, M. Fainzilber, S. di Giovanni, Reactive oxygen species regulate axonal regeneration through the release of exosomal NADPH oxidase 2 complexes into injured axons. *Nat. Cell Biol.* **20**, 307–319 (2018).
43. M. Buggisch, B. Ateghang, C. Ruhe, C. Strobel, S. Lange, M. Wartenberg, H. Sauer, Stimulation of ES-cell-derived cardiomyogenesis and neonatal cardiac cell proliferation by reactive oxygen species and NADPH oxidase. *J. Cell Sci.* **120**, 885–894 (2007).
44. F. Zhang, Y. Zhao, Z. Han, An in vivo functional analysis system for renal gene discovery in Drosophila pericardial nephrocytes. *J. Am. Soc. Nephrol.* **24**, 191–197 (2013).
45. M. Helmstadter, T. B. Huber, T. Hermle, Using the Drosophila nephrocyte to model podocyte function and disease. *Front. Pediatr.* **5**, 262 (2017).
46. H. Y. Lim, H. Bao, Y. Liu, W. Wang, Select septate junction proteins direct ros-mediated paracrine regulation of Drosophila cardiac function. *Cell Rep.* **28**, 1455–1470.e4 (2019).
47. A. Sainio, H. Jarvelainen, Extracellular matrix-cell interactions: Focus on therapeutic applications. *Cell. Signal.* **66**, 109487 (2020).
48. B. Denholm, H. Skaer, Bringing together components of the fly renal system. *Curr. Opin. Genet. Dev.* **19**, 526–532 (2009).
49. H. Agaisse, U. M. Petersen, M. Boutros, B. Mathey-Prevot, N. Perrimon, Signaling role of hemocytes in Drosophila JAK/STAT-dependent response to septic injury. *Dev. Cell* **5**, 441–450 (2003).
50. H. Yang, J. Kronhamn, J. O. Ekstrom, G. G. Korkut, D. Hultmark, JAK/STAT signaling in Drosophila muscles controls the cellular immune response against parasitoid infection. *EMBO Rep.* **16**, 1664–1672 (2015).
51. S. Chakrabarti, J. P. Dudzic, X. Li, E. J. Collas, J. P. Boquete, B. Lemaitre, Remote control of intestinal stem cell activity by haemocytes in Drosophila. *PLOS Genet.* **12**, e1006089 (2016).
52. K. Huang, T. Miao, K. Chang, J. Kim, P. Kang, Q. Jiang, A. J. Simmonds, F. di Cara, H. Bai, Impaired peroxisomal import in Drosophila oenocytes causes cardiac dysfunction by inducing upd3 as a peroxikine. *Nat. Commun.* **11**, 2943 (2020).
53. K. J. Woodcock, K. Kierdorf, C. A. Pouchelon, V. Vivancos, M. S. Dionne, F. Geissmann, Macrophage-derived upd3 cytokine causes impaired glucose homeostasis and reduced lifespan in Drosophila fed a lipid-rich diet. *Immunity* **42**, 133–144 (2015).
54. L. A. Borthwick, T. A. Wynn, A. J. Fisher, Cytokine mediated tissue fibrosis. *Biochim. Biophys. Acta* **1832**, 1049–1060 (2013).
55. Y. X. She, Q. Y. Yu, X. X. Tang, Role of interleukins in the pathogenesis of pulmonary fibrosis. *Cell Death Discov.* **7**, 52 (2021).
56. Y. Kawaguchi, Contribution of interleukin-6 to the pathogenesis of systemic sclerosis. *J. Scleroderma Relat. Disord.* **2**, S6–S12 (2017).
57. G. C. Meléndez, J. L. M. Larty, S. P. Levick, Y. Du, J. S. Janicki, G. L. Brower, Interleukin 6 mediates myocardial fibrosis, concentric hypertrophy, and diastolic dysfunction in rats. *Hypertension* **56**, 225–231 (2010).
58. E. H. Steen, X. Wang, S. Balaji, M. J. Butte, P. L. Bollyky, S. G. Keswani, The role of the anti-inflammatory cytokine interleukin-10 in tissue fibrosis. *Adv. Wound Care* **9**, 184–198 (2020).
59. D. D. Shao, R. Suresh, V. Vakil, R. H. Gomer, D. Pilling, Pivotal advance: Th-1 cytokines inhibit, and Th-2 cytokines promote fibrocyte differentiation. *J. Leukoc. Biol.* **83**, 1323–1333 (2008).
60. E. Owusu-Ansah, U. Banerjee, Reactive oxygen species prime Drosophila haematopoietic progenitors for differentiation. *Nature* **461**, 537–541 (2009).
61. M. Fink, C. Callol-Massot, A. Chu, P. Ruiz-Lozano, J. C. I. Belmonte, W. Giles, R. Bodmer, K. Ocorr, A new method for detection and quantification of heartbeat parameters in Drosophila, zebrafish, and embryonic mouse hearts. *Biotechniques* **46**, 101–113 (2009).
62. D. A. Kimbrell, C. Hice, C. Bolduc, K. Kleinhesselink, K. Beckingham, The Dorothy enhancer has Tinman binding sites and drives hopscotch-induced tumor formation. *Genesis* **34**, 23–28 (2002).
63. P. Georgel, S. Naitza, C. Kappler, D. Ferrandon, D. Zachary, C. Swimmer, C. Kopczynski, G. Duyk, J. M. Reichhart, J. A. Hoffmann, Drosophila immune deficiency (IMD) is a death

domain protein that activates antibacterial defense and can promote apoptosis. *Dev. Cell* **1**, 503–514 (2001).
64. T. Sandmann, L. J. Jensen, J. S. Jakobsen, M. M. Karzynski, M. P. Eichenlaub, P. Bork, E. E. M. Furlong, A temporal map of transcription factor activity: Mef2 directly regulates target genes at all stages of muscle development. *Dev. Cell* **10**, 797–807 (2006).
65. S. A. Sinenko, T. Hung, T. Moroz, Q. M. Tran, S. Sidhu, M. D. Cheney, N. A. Speck, U. Banerjee, Genetic manipulation of AML1-ETO-induced expansion of hematopoietic precursors in a Drosophila model. *Blood* **116**, 4612–4620 (2010).
66. E. Kuranaga, H. Kanuka, T. Igaki, K. Sawamoto, H. Ichijo, H. Okano, M. Miura, Reaper-mediated inhibition of DIAP1-induced DTRAF1 degradation results in activation of JNK in Drosophila. *Nat. Cell Biol.* **4**, 705–710 (2002).
67. F. Zhou, A. Rasmussen, S. Lee, H. Agaisse, The UPD3 cytokine couples environmental challenge and intestinal stem cell division through modulation of JAK/STAT signaling in the stem cell microenvironment. *Dev. Biol.* **373**, 383–393 (2013).
68. K. Tsuneizumi, T. Nakayama, Y. Kamoshida, T. B. Kornberg, J. L. Christian, T. Tabata, Daughters against dpp modulates dpp organizing activity in Drosophila wing development. *Nature* **389**, 627–631 (1997).
69. L. Zhang, F. Ren, Q. Zhang, Y. Chen, B. Wang, J. Jiang, The TEAD/TEF family of transcription factor Scalloped mediates Hippo signaling in organ size control. *Dev. Cell* **14**, 377–387 (2008).

Acknowledgments: We thank E. Bach, J.A. Hoffmann, S. Newfeld, T. Tabata, E. Chen, U. Banerjee, M. Miura, and J. Jiang for reagents; Bloomington Drosophila Stock Center and Kyoto Stock Center DGRC for fly stocks; Developmental Studies Hybridoma Bank for antibodies; other members of the laboratory for critical input; and IISER Mohali confocal (Leica SP8) facility for imaging. The models were created using BIORENDER. **Funding:** This study was funded by IISER Mohali (J.G.), CSIR, India (P.B. and M.S.), Department of Science and Technology, India (EMR/2016/001519 and CRG/2020/000511) (S.M.), and Wellcome Trust DBT India Alliance, India (IA/S/17/1/503100) (L.M.). **Author contributions:** Conceptualization: S.M. Methodology: J.G. and P.B. Investigation: S.M., J.G., P.B., and M.S. Visualization: J.G. Supervision: S.M. Writing—original draft: S.M. Writing—review and editing: S.M., J.G., P.B., and L.M. **Competing interests:** The authors declare that they have no competing interests. **Data and materials availability:** All data needed to evaluate the conclusions in the paper are present in the paper and/or the Supplementary Materials.

Submitted 17 May 2021
Accepted 23 December 2021
Published 18 February 2022
10.1126/sciadv.abj4991